Computational and Theoretical Chemistry 1212 (2022) 113709

Contents lists available at ScienceDirect

Computational and Theoretical Chemistry

journal homepage: www.elsevier.com/locate/comptc

Toxic potential of Poly-hexamethylene biguanide hydrochloride (PHMB): A DFT, AIM and NCI analysis study with solvent effects

Sibel Celik [a,*], Emine Tanıs [b]

[a] Vocational School of Health Services, Kırsehir Ahi Evran University, 40100 Kırşehir, Turkey
[b] Department of Electrical Electronics Engineering, Kırsehir Ahi Evran University, 40100 Kırsehir, Turkey

ARTICLE INFO

Keywords:
Poly(hexamethylene biguanide) Hydrochloride
Solvent effect
DFT
Toxic potential
AIM

ABSTRACT

In the current study, the toxic material Poly-hexamethylene biguanide hydrochloride (PHMB) has been characterized by UV–Visible and infrared spectroscopy in different solvent environments. The nature of the molecular interactions between solvent molecules and PHMB via hydrogen bonds has been investigated using the Atoms in Molecules (AIM) and non-covalent reduced density gradient (NC-RDG) analyses. Intermolecular interactions are further supported by the Natural Bond Orbital (NBO) analysis, which was carried out to provide information about the delocalization of charge and energy density of the atoms. The O—H···Cl and N—H···Cl hydrogen bond types of interaction in solvent complexes have indicated weak hydrogen bonds. Moreover, we studied the endocrine disrupting potential of PHMB by using *VirtualToxLab* technology.

1. Introduction

Poly-hexamethylene biguanide hydrochloride / polyhexanide / polyaminopropyl biguanide (PHMB; CAS No: 32289–58-0), a member of the antiseptic bioguanides, is a polymer possessing biocidal effects, including antimicrobial activity [1-3]. Due to its biocidal activities, it has been used as preservative for several products such as food, fabric softeners, personal care products, water treatment agents, and surface disinfectants [3,4]. Even though it was announced as safe with a low risk of adverse health effects by the US Environmental Protection Agency (EPA), it has limited usage (up to a maximum concentration of 0.3%) in cosmetics and is considered unsafe in cosmetics that are in spray form as it is considered to have acute toxicity when inhaled [5]. It is known that PHMB has antimicrobial activity on yeast, bacteria, amoebae and also human immunodeficiency virus type-1 [6-8].

The biocidal activity of PHMB depends on the physical disruption of the membranes of target cells, so it can be said that it is a membrane-active biocide. It is reported to be useful against multidrug-resistant bacteria due to its preventative action on bacterial envelope development [9]. It attaches to the anionic phospholipids of the bacterial membrane and affects the membrane stability [10,11].

PHMB is used as antiseptic at hospitals and also found to be useful for burns and chronic wounds [9,12-14]. Additionally, PHMB is suggested to be impregnated to gloves in order to prevent or reduce the healthcare-associated infections [15]. Even though, PHMB containing products are widely marketed and used as antiseptics, the risk assessment process for them is still on going. Currently, its label as approved by the European Union is "fatal if inhaled, causes damage to organs through prolonged or repeated exposure, is very toxic to aquatic life, is very toxic to aquatic life with long lasting effects, is harmful if swallowed, causes serious eye damage, is suspected of causing cancer, and may cause an allergic skin reaction" [16].

Besides beneficial effects, it has been reported that PHMB is toxic to human keratocytes while treating a serious eye infection, namely Acanthamoeba keratitis [17]. Moreover, PHMB has been shown to increase liver tumor incidence when doses in excess of the maximum tolerated dose are administered to the drinking waters of rats. The mode of action of this effect has also been investigated, but no cytotoxic effect in the liver has been found and it has been reported that PHMB may cause increased cell proliferation [18]. Like all biocidal disinfectants, PHMB occurs in the aquatic environment and its effects on aquatic organisms are yet to be known. The only study has been done on zebrafish liver cell lines, and low cytotoxicity has been found [19].

The effects of PHMB on the endocrine system have not been investigated and are still unknown. Recently, a program, named *VirtualToxLab,* has been reported to check the binding affinities of chemicals to biologically important proteins. It enables to estimate the toxic potential of chemicals, natural products, and drugs. This *in silico* technology is

* Corresponding author.
E-mail address: sibelcelik@ahievran.edu.tr (S. Celik).

https://doi.org/10.1016/j.comptc.2022.113709
Received 10 March 2022; Received in revised form 10 April 2022; Accepted 11 April 2022
Available online 14 April 2022

based on an automated procedure mimicking the interaction of chemicals with 16 proteins [20]. Here, we investigated for the first time the endocrine disrupting potential of PHMB by using *VirtualToxLab* technology.

Solvation effects are very important in deciding the functionability and activity of a compound in a medium, especially inside the body of living things [21]. Solvents affect the solubility, stability, and rate of thermodynamic and kinetic control processes. Solvent effect-based stability, hydrogen bond formation between solvent and solute, dipole–dipole interactions, and van der Waals interactions. Solvents exhibit cluster features and also biological activity [22]. As a result of these considerations, the purpose of this paper is to investigate the interaction of PHMB with solvents.

This research is divided into two sections. The first part investigates the spectroscopic and energetic features of the solvent effects on the PHMB compound in solution, while the second part investigates the PHMB-solvent complexes interactions. The Uv–Vis and FT-IR spectra were investigated theoretically and experimentally in solutions (ethanol, methanol, DMSO, water). FT-IR spectra are a major technique for studying molecular vibrations. Since vibrational frequency changes of solute molecules in solution reflect solute–solvent interactions, they have also been used to investigate the effects of solvents. Attention has been paid to the hydrogen bond cooperation effect and the nature of interactions between solvent molecules using binary energy calculation, atoms in molecules (AIM), and non-covalent interactions-low density gradient (NCI-RDG) analysis. Furthermore, the Natural Bond Orbital (NBO) analysis explains the delocalization of the charge between the PHMB and the solvent molecule. The NBO search was measured in redistribution in various (bond and anti-bond) orbitals and stabilization energies.

2. Materials and methods

2.1. Experimental studies

PHMB was purchased from Aldrich and used without further purification. The FTIR spectra and UV–Vis absorption spectra of PHMB in solution (ethanol, methanol, DMSO, water) were recorded. The FTIR spectra were registered using a Mattson 1000 FTIR spectrometer within the wavelength range of 400–4000 cm^{-1} and the assignments of all the observed bands were made with 0.2 cm^{-1} resolution. UV–Vis absorption spectra are recorded in the 200–600 nm range by using a Thermo Scientific spectrophotometer.

2.2. Theoretical methods

2.2.1. Computational details

The calculations were carried out by using the Gaussian 09 program package [23] and the GaussView molecular visualization program [24]. Vibrational wavenumbers and energy analysis of PHMB in different solvents were also calculated at the DFT/B3LYP/6–311++G(d,p) level of theory. Solute–solvent effects were taken into account by employing the self-consistent reaction field (SCRF) method based on the polarizable continuum model (PCM) developed by Tomasi et al. [25]. Global reactivity descriptors such as HOMO-LUMO gaps and chemical hardness, electronegativity, chemical potential, and electrophilicity index were calculated for PHMB-solvent complexes. These parameters are obtained using the DFT/B3LYP/PCM/6–311++G(d,p) level. The Gauss view 5.0 software was used to obtain the highest occupied and lowest unoccupied molecular orbital maps (HOMO-LUMO) and molecular electrostatic potential maps for identifying the potential region [26]. NBO analysis was done on a molecule at the same level using second order Fock to show that the stabilization comes from hyperconjugation of various intramolecular interactions. The NBO analysis was carried out using the NBO 3.0 software [27], which is included in the Gauss 09 package. Using the Multiwfn software based on the quantum theory of AIM, the H-bond interactions were described in terms of electron density, ρ(r), its Laplacian $\nabla^2\rho(r)$ and potential energy density at ring critical points (BCP) [28,29]. By employing Multiwfn [28] and the molecular visualization program VMD [30], RDG analysis provided an easy-to-catch pictorial visualization of different kinds of non-covalent interactions directly in real space. The PHMB from the ground state at the TD-DFT/B3LYP/6–311++G(d,p) level of theory was used to calculate the excited states to achieve theoretical UV–Vis spectra in different solvents.

2.2.2. VirtualToxLab analyses

Toxic potential of PHMB (Fig. S1) was determined using *VirtualToxLab* which enables to estimate the toxic potential by using binding affinities of agents towards 16 biologically important proteins namely androgen receptor (AR), estrogen receptor α (ERα), estrogen receptor β (ERβ), glucocorticoid receptor (GR), liver X receptor (LXR), mineralocorticoid receptor (MR), peroxisome proliferator-activated receptor γ (PPAR γ), progesterone receptor (PR), thyroid receptor α (TRα), thyroid receptor β (TRβ), four cytochrome P450 enzymes (CYP1A2, CYP2C9, CYP2D6, CYP3A4), aryl hydrocarbon receptor (AhR) and potassium ion channel (hERG). This *in silico* technology combines mQSAR and docking to quantify the binding affinities. The values of toxic potential range from 0.0 (none) to 1.0 (extreme) [20,31]. Here, the toxic potential and binding affinity (IC_{50} nanomolar) of PHMB towards 16 proteins suspected to trigger endocrine and metabolic disruption were determined. Binding affinity greater than 100 μM was accepted as “not binding”.

3. Results and discussion

3.1. Energy analysis in solvent

The molecular dipol moment (μ) is particularly sensitive to the solvent dielectric constant (ε). The dipol moments of PHMB obtained by means of the DFT calculations are portrayed in Table 1. The results pointed out that the dipol moment was increased by changing the gas phase to the solution, as well, by increasing the solvent polarity. Generally, the dielectric constant of the solvent provides a rough measure of the solvent’s polarity.

The calculated total energies (E^{tot}), relative energies (ΔE) and stabilization energy ($E_{solvation}$) for PHMB were compared and analyzed in the gas phase and in various solvents. A decrease was observed at the total energies for PHMB as the solvent polarity increased (ethanol = −1049.84520158 a.u, methanol = −1049.84536564 a.u, DMSO = −1049.84552806 a.u, water = −1049.84568073 a.u). As shown in Table 1, structure of PHMB had the lowest energy in each medium when moving from gas phase to solvent (ethanol to methanol to DMSO to water) on a negative continuum. The dipole in the molecule will induce a dipole in the medium. Besides, an electric field applied to the solute by the solvent (reaction) dipole will in turn interact with the molecular dipole to lead to net stabilization. The stabilization energy by solvents was calculated as follows; $E_{solvation} = E_{in\ solvent} – E_{in\ gas.}$ The $E_{solvation}$ is the stabilization energy by solvents, the relative energy of complex in a solvent to that in the gas phase. The stabilization energy of the solvent was used to evaluate the interaction strength of molecule with the solvent. In terms of the energies, E^{tot} showed a decrease with the increasing dielectric constants of solvents, and $E_{solvation}$ increased due to the solvent

Table 1
Solvation energies ([a]ΔE_s), solvation free energies ([b]ΔG_s), and dipol moments μ (in debye) of the PHMB in gas phase and different solvents.

	ε = 1	ε = 24.5	ε = 32.7	ε = 46.7	ε = 80.1
[a]ΔE_s	0	−23.3032	−23.7339	−24.1603	−24.5612
[b]ΔG_s	0	−25.7141	−26.1946	−26.9998	−27.1109
μ	1.1299	1.3109	1.3147	1.3188	1.3230

[a] $\Delta E_s = E_{solution} - E_{gas}$ (in kJ/mol).
[b] $\Delta G_s = G_{solv} - G_{gas}$ (in kJ/mol).

effect.

Calculated ΔG_{solv} of the PHMB were listed in Table1. It can be found that the ΔG_{solv} value increased with the rise of the solvent polarity, and thus, the solvation of PHMB increased with the polarity of the solvent. The value of ΔG_{water} was more negative than that of ethanol, methanol, and DMSO, which means that the solvation of PHMB in water was better than in other solvents. The very high solubility of PHMB in water (>40% w/w) is proof of the high hydration enthalpy [2]. The computed ordering of the solvation free energies in several solvents was as follows: water > DMSO > methanol > ethanol.

These results suggested that PHMB was easy to dissolve in polar solvents and remained more stable in more polar solvents. The change in dipole moments was in accordance with the changes in charge distributions and molecular geometry in going from the gas-phase to solution.

3.2. Vibrational frequencies in solvent

The computed wavenumber shifts in different solvents with respect to the gas phase are given in Table S1. The computed wavenumbers in the phase and in solvents were all scaled by a factor of 0.9978. The DFT calculated frequencies in the solvent phase were obtained using the PCM model at the B3LYP/6–311++G(d,p). The experimental IR spectra in liquid phase were given in (Fig S2). The IR intensities were calculated from the gas phase to different dielectric media. The solvent effect on the frequency difference $\Delta\nu$ between those in the gas phase and those in solvents was tabulated in Table S1. Changes in vibrational modes were obtained as significant when moving from the gas phase to solution.

In the study by Rodrigues et al. [32], the experimental and theoretical FT-IR of the PHMB molecule were investigated. The experimental spectrum showed ν(NH) bands between 3290 and 3400 cm^{-1}. The amino group (NH_2) stretching vibration usually occurs in the range of 3500–3300 cm^{-1} [33]. In the region between 3100 and 3350 cm^{-1} of the experimental IR spectrum, the ν(NH), was in agreement with the literature [34-36]. In our study, NH stretching vibrations in different solvents shifted to 3418 and 3184 cm^{-1} in ethanol, 3418 and 3165 cm^{-1} in methanol, 3430 and 3012 cm^{-1} in DMSO, and cm^{-1} in water. The presence of solvent groups interacting with this protonated region resulted in a stronger intramolecular H-bond and a stronger downshifting effect. The aromatic CH stretching vibration wavenumbers calculated in the expected ranges with previous studies [37,38] are in the range of 3100–2700 cm^{-1} and large shifts were observed in the solvent.

The characteristic absorption peaks for PHMB were observed at 1650 cm^{-1} and about 1587 cm^{-1} attributed to C═N stretching and bend vibration of NH_2^+ [39]. When the experimental frequencies for this area were compared, in all solvents, the peak at 1587 cm^{-1} shifted to 1555 cm^{-1}, whereas the peak at 1650 cm^{-1} was detected at 1648 cm^{-1} (strong) in ethanol and 1655 cm^{-1} (weak) in methanol and DMSO. The C—N stretch appearing between 1000 and 1200 cm^{-1} [32,38] was seen in this study as downshifted strong bands in the solvent.

The most important bonds were those located in the 2000–2400 cm^{-1} range, corresponding to nitrogen-related vibrations, including combination bands due to nitrogen-carbon bonds in the biguanide pseudo-aromatic ring. The remaining bonds were due to methylene groups and residual hydration water. Bands associated with chlorine ion were not present, but the -bonded behavior of some vibrations may be due to chloride interference on —N—H vibrations [2].

For instance, comparison of $\Delta\nu$ between gas phases in solvent at the largest change was observed for ν_6, ν_9, ν_{10}, ν_{11}, ν_{14}, ν_{16} ν_{17} modes. The average change of frequencies ($\Delta\nu$) remained nearly the same the trend from ethanol to water.

3.3. The absorption characteristics of the PHMB in the solvent

The experimental absorbance results of the PHMB in solution (DMSO/ethanol/methanol and water) are shown in Fig. 1. PHMB material gave absorbance peaks at 283 nm with different absorbance intensities in all solvents. In addition, it is seen that our results are also compatible with the literature [5]. It is understood from these results that PHMB has maximum absorbance peaks in the middle-UV region for all solvents. Furthermore, the absorption of the PHMB material does not change in the related solvents.

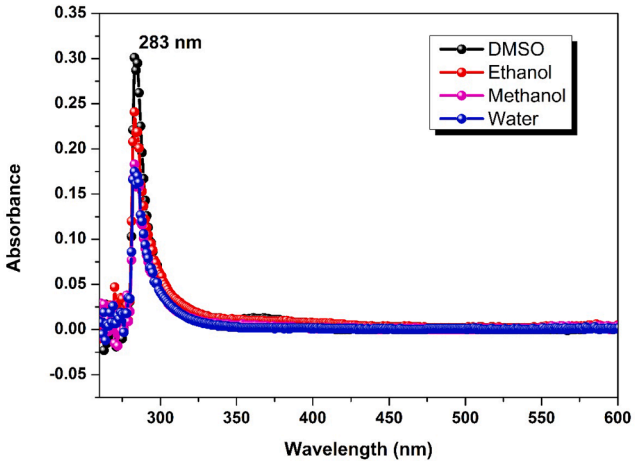

Fig. 1. The experimental UV–Vis absorption spectra of PHMB in solvents.

In order to determine the electronic properties of a molecule, it is necessary to examine the electronic transitions from, σ, π, n ground state orbitals to σ*, π*, n* excited states [40]. For this, ultraviolet spectroscopy of PHMB molecule in gas and solutions was calculated using the TD-DFT/B3LYP/6–311++G(d,p) level of theory and is listed in Table S2. From the table, it is seen that the highest absorption peak occurred in the gas phase at a wavelength of 301 nm, between the HOMO → LUMO orbitals, with a band gap value of 4.11 eV. Absorption peak values for solvents are the same, occurring at 211 nm, 209 nm and 208 nm.

3.4. HOMO-LUMO analysis and chemical descriptors of PHMB-solvent complexes

The gap between the highest occupied molecular orbital and the lowest unoccupied molecular orbital, E_{gap}, and global rectivity descriptors such as Electron affinity (A), Ionization energy (I), Chemical hardness (η) and softness (σ), Electronegativity (χ), Chemical potential (μ) and the Electrophilicity index (ω) play an important role in chemical reactions as well as electrical and optical performance [41]. These parameters, obtained using the DFT/B3LYP/6–311++G (d,p) level of theory, are tabulated in Table 2 Fig. 2. Koopman [42] defines closed shell components η, μ, and χ as $\eta = I\text{-}A$, $\mu=(I\text{-}A)/2$, $\chi=(I + A)/2$, $\omega = \mu^2/2\eta$. Electron affinity and ionization potential can be estimated through HOMO and LUMO orbital energies as $A = -E_{LUMO}$ and $I = -E_{HOMO}$. The electronegativity and chemical hardness are often used to make chemical reactivity prediction. Also, a molecule with a small frontier orbital gap is called a soft molecule. Soft molecules are more polarizable and have a high chemical reactivity as well as low kinetic stability [43,44]. Rodrigues et al. [32] HOMO-LUMO energy gap calculations using both the B3LYP/6–31++(d,p) (5.33 eV) and M06-2X/6–31++(d,p) (7.55 eV) functionals showed that PHMB is an electrical insulator as it has a large HOMO-LUMO energy gap. In the present study, the E_{gap} value calculated in the gas phase with the B3LYP/6–311++G(d,p) method was 4.76 eV. In both studies, there is a large energy barrier separating these orbitals, and HOMO-LUMO electronic transitions are difficult to occur in PHMB. The lowest energy band gap was calculated for the DMSO complex, (4.29 eV) and the highest energy band gap was calculated for the water complex (4.82 eV). Therefore, it can be said that the PHMB-H_2O complex had higher chemical stability than the other

Table 2
Calculated HOMO-LUMO energy gaps and quantum chemical properties of the PHMB-solvent complexes.

Parameters	In gas	PHMB···EtOH	PHMB···MeOH	PHMB···DMSO	PHMB···H2O
$E_{HOMO-1-LUMO+1\ gap}$ (eV)	5.01	6.68	6.68	6.18	6.55
$E_{HOMO-LUMO\ gap}$(eV)	4.76	4.81	4.81	4.29	4.82
Chemical hardness (η) (eV)	2.38	2.40	2.40	2.15	2.41
Global softness (σ) (eV) $^{-1}$	0.21	0.20	0.20	0.23	0.21
Electronegativity (χ) (eV)	3.19	3.97	3.97	3.87	3.95
Chemical potential (μ) (eV)	−3.19	−3.97	−3.97	−3.87	−3.95
Electrophilicity index (ω) (eV) $^{-1}$	−2.14	−3.28	−3.28	−3.49	−3.23

solutions. In solvent with a large dielectric constant, the solvent–solute interaction is more stabilized due to hydrogen bonding and dipole–dipole interactions [45,46]. Water is the solvent with the largest dielectric constant and polarity among the other solvents studied. The larger the HOMO-LUMO energy gap value, the greater the stability of the molecule. Therefore, we can say that our result is in parallel with the literature. It is understood from the table that the chemical hardness value was the highest and the lowest electrophilicity value was at the PHMB-H_2O complex.

3.5. AIM topological, reduced density gradient (RDG) and NBO analyses of PHMB-solvent complexes

The AIM (Atoms In Molecules) approach involves specifying the many characteristics of chemical bonds, such as hydrogen bonds [47]. This method is commonly used to calculate inter-atomic and intra-atomic interactions. The electron density ρ(r), the Laplacian $\nabla^2\rho(r)$, the eigenvalues (λ_1, λ_2, λ_3), the kinetic energy densities G(r), the total energy densities H(r), the potential V(r) and the bond energy E_{HB} are all topological characteristics providing much information. The AIM theory is commonly used to examine chemical bond characteristics, especially hydrogen bonds. The hydrogen-bonds and their notions are well described by the AIM theory. According to Rozas et al. [48], hydrogen bond interactions can be classified as follows:

- Strong H-bonds are characterized by $\nabla^2\rho(r) < 0$, $H(r) < 0$, $E_{HB} > 100$ kj/mol and their covalent character is established.
- Moderate H-bonds are defined by $\nabla^2\rho(r) > 0$, $H(r) < 0$, $50 < E_{HB} <$ 100 kj/mol and their partially covalent character.
- The weak H-bonds are characterized by $\nabla^2\rho(r) > 0$, $H(r) > 0$, $E_{HB} <$ 50 kj/mol and they are mainly electrostatic, with a distance between the interacting atoms greater than the sum of their van der Waals rays [49,50].

The intramolecular BCPs and ring critical points (RCPs) between PHMB and EtOH, MeOH, DMSO, and H2O molecules were obtained using the optimized PHMB-solvent complexes for AIM studies. In this work, the following topological descriptors were utilized to determine the nature of the hydrogen-bond between the investigated PHMB and solvents. Fig. 3 depicted the graphical representation of the AIM analysis of PHMB-solvent complexes, while Table 3 listed the calculated topological parameters. As shown in Fig. 3, the interactions between the biguanide aromatic ring and the solvent molecules via hydrogen bonds gave rise to the formation of the rings NRCP. In PHMB-solvent complexes, O—H···Cl, N—H···Cl and N—H···O interactions between ligand and solvent molecules were detected as intermolecular interactions, whereas N—H···N interactions were observed as intramolecular interactions (see Fig. 3).

According to Table 3, strong hydrogen bond interactions in the PHMB···(H2O) complex had a negative laplacian $\nabla^2\rho(r)$ and a negative total energy density H(r) at the O—H···Cl of binding was indicative of a strong covalent character. Also, N—H···Cl had lower values of $\rho(r)$ and E_{HB} than the other two H-bonds, N3-H15···O and N1-H18···N5, indicating that this bond is weaker. The hydrogen bond types (O—H···Cl, N—H···Cl) of interaction in other solvent complexes had a positive laplacian and total energy densities, indicating weak hydrogen bonds. The N—H···N hydrogen bond in PHMB···(dimethyl sulfoxide/ethanol/methanol) complexes had a moderate hydrogen bond character, since it had a positive laplacian and a negative total energy density. The computed interaction energies for the PHMB···(H2O) complex were considered the strongest interactions with hydrogen bond energies among the PHMB-solvent complexes, indicating that the intermolecular bond strength was strong in this complex.

The NCI analysis provides important information regarding a molecule's non-covalent interactions. Noncovalent interactions (NCI) method developed by Johnson et al. assesses the molecular bonding and nonbonding interaction regions by the reduced density gradient (s) [51,52], which is described by.

$$s = \frac{1}{2(3\pi^2)^{1/3}}\left(\frac{|\nabla^2\rho(r)|}{\rho(r)^{4/3}}\right)$$

The noncovalent interaction (NCI) analysis was used to illustrate the interactions using graphical representations in real space. The examined system had a somewhat weaker hydrogen bond, as mentioned in the hydrogen bond AIM analysis, resulting in a tiny negative value. RGD points plotted against electron density multiplied by the sign of second eigenvalue (sign(λ2)ρ) (left) and NCI plot (right) were shown in Fig. 4, with the strong intermolecular interaction of each PHBM-solvent complex. The isosurfaces use color codes to represent the many types of NCI in actual space. Strong attraction (H-bonding), weak interaction (van der Waals attraction), and strong repulsion (steric repulsion) were shown by the colors blue, green, and red, respectively. Figure showing the properties of H-bond interaction in the PHMB-solvent complexes are represented by blue colored isosurfaces. N—H···Cl interaction showed by green color in all complexes, representing weak intermolecular interactions. The steric effect presented in the ring due to high repulsions in all complexes was indicated by the red colored isosurface. These results were comparable to those found using the AIM method.

The Natural Bonding Orbital (NBO) method was used to analyze the H-bonding interactions between a wide range of chemical systems [53]. The interaction between donor and acceptor in the NBO analysis was characterized by a stabilization energy $E^{(2)}$, where qi, F(i,j), and εi, εj indicate the occupation of the orbital i the Fock matrix element outside the diagonal, and the diagonal elements, respectively. The value of stabilization energy was proportional to the degree of the interaction between donor and electron acceptor; the greater the value of $E^{(2)}$, the more intense the interaction between donor and electron acceptor was observed. Table 4 lists the selected values of the calculated second order interaction energy $E^{(2)}$ of H-bonds in the investigated PHMB-solvent. As seen in the table, the highest stabilization energy, equal to 27.87 kcal/mol, was in PHMB–H_2O. We can see this interaction in the strong anionic-cationic group interaction, which was formed in the hydrogen bonding of O34-H26…Cl, between the pair of LP(Cl) orbitals and the σ* (O34-H26) antibonding orbital. In all complexes, the interaction $LP(1)(N_5)\rightarrow\sigma^*(N_1 - H_{18})$ in the biagudin ring had the highest perturbation energies, $E^{(2)}$ providing a stronger stabilization to the structure than the other interactions. Furthermore, N—H….Cl hydrogen bonds were weak, and this was confirmed by the low value of the energy $E^{(2)}$ assigned as LP → σ* interaction system. All of these NBO results were

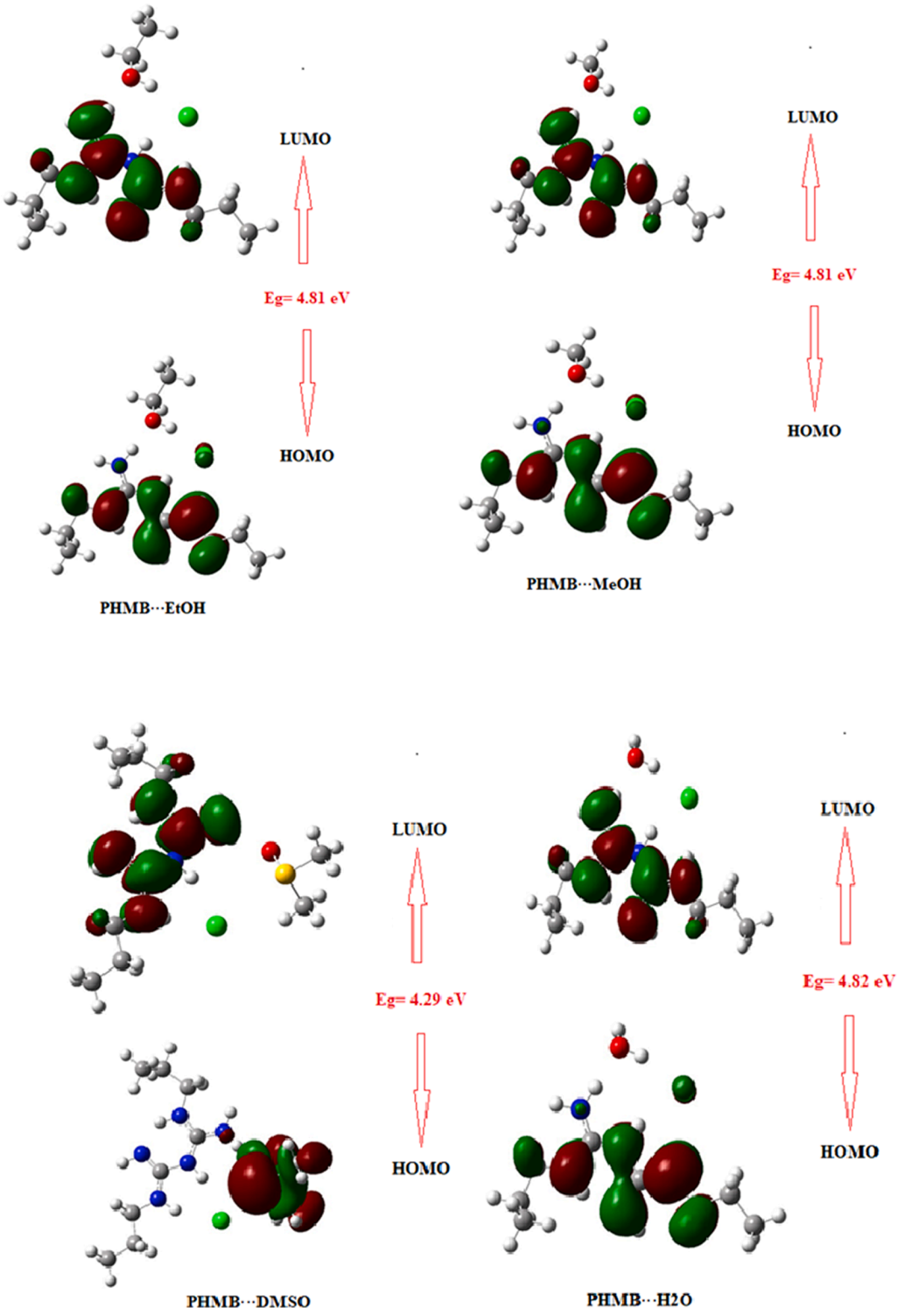

Fig. 2. HOMO-LUMO diagram of the PHMB-solvent complexes.

consistent with the AIM topological and NCI analysis.

3.6. *VirtualToxLab analyses*

Toxic potential of PHMB was found as 0.055 indicating that PHMB was a non-toxic compound according to *VirtualToxLab* analysis. It also showed no binding to any of the proteins checked.

4. Conclusions

In this work, the solvent effects of PHMB were investigated by FTIR, absorbance spectra, DFT, RDG, NBO, and VirtualToxLab analysis. It was understood that the chemical stability of PHMB was highest in the PHMB-H2O complexes. There was no notable change in the frontier molecular orbitals and energy gap in the transition from the gas phase to

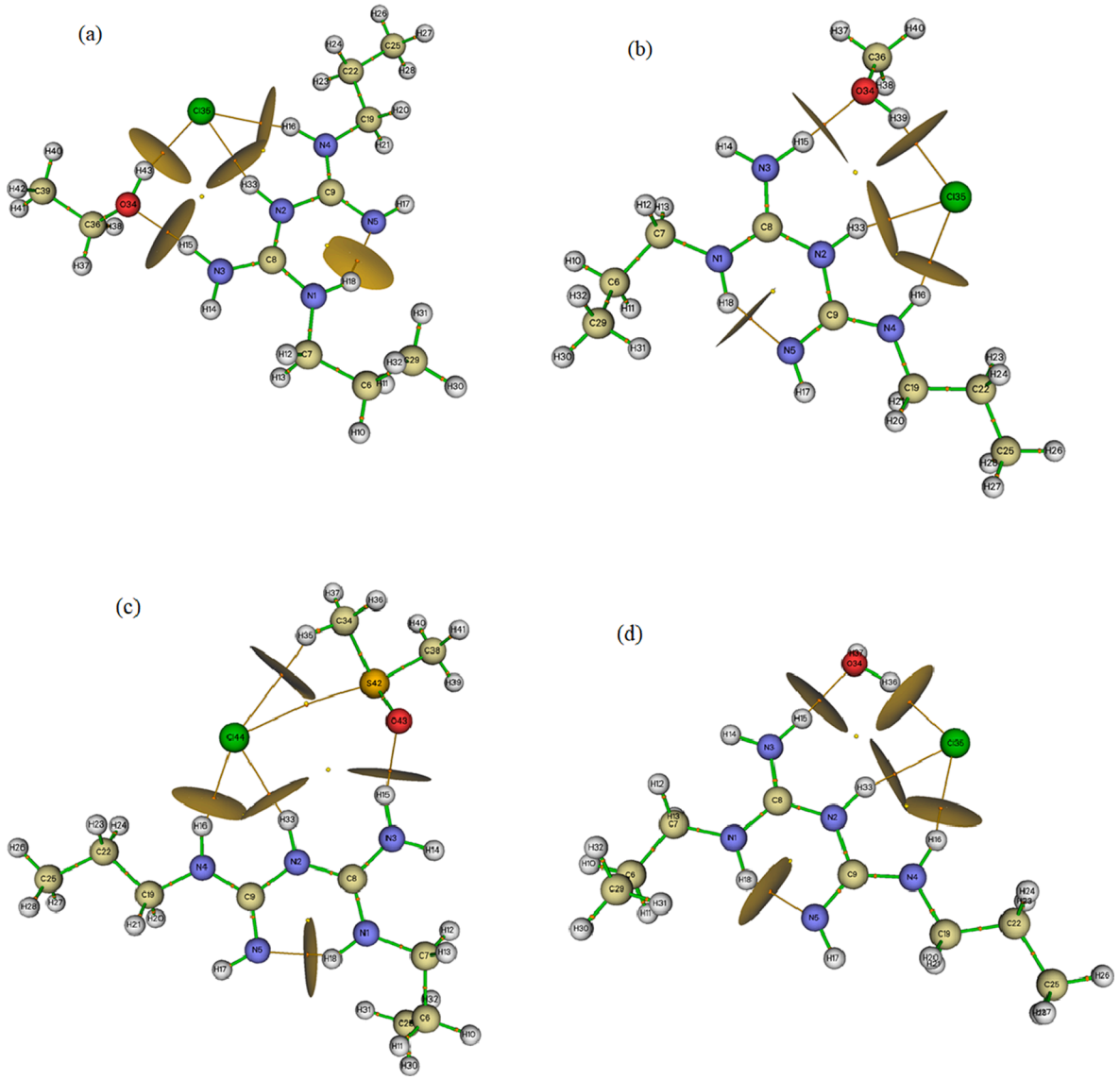

Fig. 3. AIM analysis of the different critical points representing H-bonds between (a) PHMB – ethanol, (b) PHMB – methanol, (c) PHMB – DMSO and (d) PHMB – water.

Table 3
Topological parameters of hydrogen bonded interaction for PBHM-solvent complexes.

	Interactions	$\rho(r)$	$\nabla^2\rho(r)$	$H(r)$	$G(r)$	$V(r)$	E_{bond}(kJ/mol)	λ_1	λ_2	λ_3
PHMB-EtOH	O_{34}-H_{43}….Cl	0.02246	0.06399	0.00002	0.01597	−0.01594	20.92	−0.00302	−0.02951	0.12376
	N_2-H_{33}….Cl	0.01898	0.05465	0.00157	0.01201	−0.01052	13.80	−0.02077	−0.02045	0.09588
	N_4-H_{16}….Cl	0.01670	0.05066	0.00189	0.01077	−0.00887	11.64	−0.01754	−0.01716	0.08536
	N_3-H_{15}….O	0.03199	0.10991	0.00016	0.02681	−0.02614	34.30	−0.05252	−0.04980	0.21224
	N_1-H_{18}…. N_5	0.04050	0.11662	−0.00308	0.03224	−0.03086	40.50	−0.06300	−0.06113	0.24075
PHMB-MeOH	O_{34}-H_{39}….Cl	0.02595	0.06535	−0.00429	0.01679	−0.01719	22.56	−0.03246	−0.03168	0.12951
	N_2-H_{33}….Cl	0.01827	0.05382	0.00168	0.01162	−0.00993	13.03	−0.01974	−0.01940	0.09242
	N_4-H_{16}….Cl	0.01663	0.05051	0.00191	0.01107	−0.08807	115.59	−0.01745	−0.01710	0.08507
	N_3-H_{15}….O	0.03204	0.10971	0.00064	0.02678	−0.02613	34.29	−0.05273	−0.04997	0.21243
	N_1-H_{18}…. N_5	0.04068	0.11678	−0.00318	0.03237	−0.03556	46.67	−0.00302	−0.06151	0.24171
PHMB-DMSO	C_{34}-H_{35}….Cl	0.00629	0.01948	0.00103	0.00383	−0.01028	13.49	−0.00483	−0.00460	0.28923
	N_2-H_{33}….Cl	0.01984	0.05634	0.00141	0.01267	−0.01127	14.79	−0.02205	−0.02171	0.10011
	N_4-H_{16}….Cl	0.01967	0.05644	0.00143	0.01126	−0.01112	14.59	−0.02167	−0.02138	0.09951
	N_3-H_{15}….O	0.03529	0.11881	−0.00038	0.03529	−0.03047	39.99	−0.05737	−0.05495	0.23112
	N_1-H_{18}…. N_5	0.04124	0.11773	−0.03427	0.03286	−0.03629	47.63	−0.06445	−0.06262	0.24490
PHMB-H_2O	O_{34}-H_{36}….Cl	0.30457	−0.19842	−0.53495	0.03889	−0.57384	753.16	−0.13591	−0.13189	0.69387
	N_2-H_{33}….Cl	0.01808	0.05285	0.00171	0.01149	−0.00978	12.83	−0.01949	−0.01917	0.09151
	N_4-H_{16}….Cl	0.01657	0.05036	0.00191	0.01067	−0.00875	11.48	−0.01737	−0.01701	0.08475
	N_3-H_{15}….O	0.02911	0.10395	0.00156	0.02445	−0.02291	30.06	−0.04646	−0.04412	0.19455
	N_1-H_{18}…. N_5	0.04061	0.11675	−0.00313	0.03232	−0.03546	46.54	−0.06324	−0.06361	0.24133

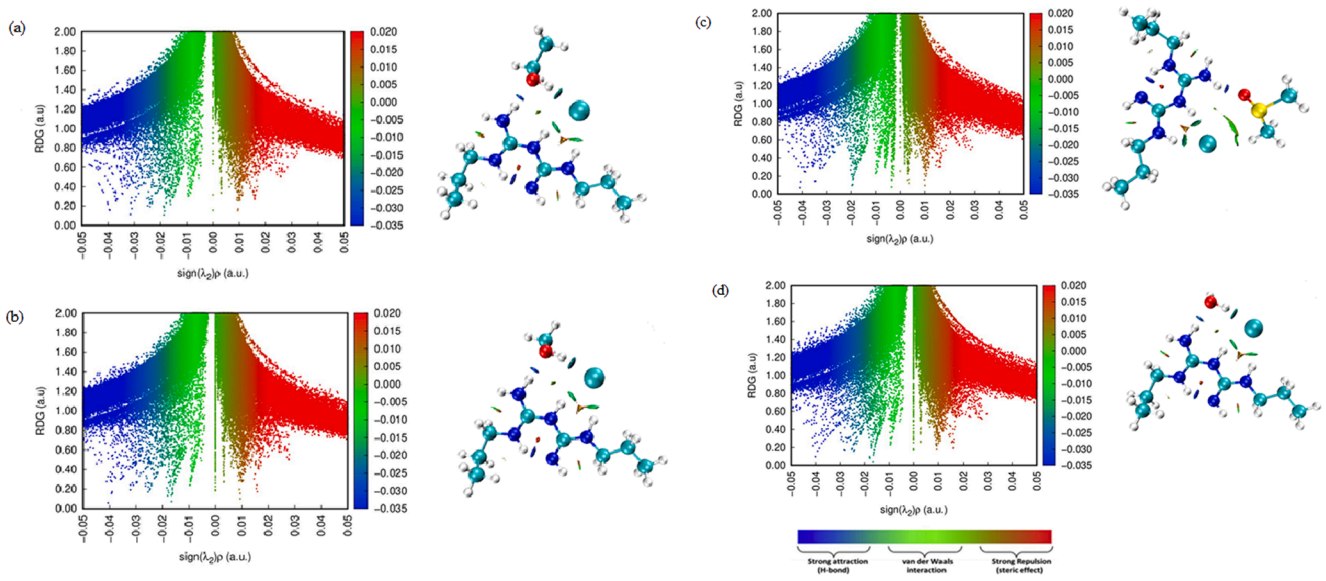

Fig. 4. RDG scatter plots (left) and corresponding non-covalent interaction (NCI) plots (right) of (a) PHMB – ethanol, (b) PHMB – methanol, (c) PHMB – DMSO and (d) PHMB – water. The isosurfaces were colored (right) with respect to the values of sign (λ2)ρ (a.u.).

Table 4
Some selected second-order H-bonds interaction energies for the PHMB-solvent complexes.

	H-bonds	*donor → acceptor*	$E^{(2)}(kcal/mol)^a$	$\varepsilon_j - \varepsilon_i(a.u.)^b$	$F(i,j)(a.u.)^c$
PHMB-EtOH	O_{34}-H_{43}….Cl	$LP(4)(Cl) \rightarrow \sigma^*(O_{34} - H_{43})$	13.03	0.77	0.078
	N_2-H_{33}….Cl	$LP(4)(Cl) \rightarrow \sigma^*(N_2 - H_{33})$	11.13	0.72	0.068
	N_4-H_{16}….Cl	$LP(3)(Cl) \rightarrow \sigma^*(N_4 - H_{16})$	8.43	0.69	0.068
	N_3-H_{15}….O	$LP(2)(O) \rightarrow \sigma^*(N_3 - H_{15})$	17.13	0.82	0.106
	N_1-H_{18}…. N_5	$LP(1)(N_5) \rightarrow \sigma^*(N_1 - H_{18})$	22.88	0.79	0.121
PHMB-MeOH	O_{34}-H_{39}….Cl	$LP(4)(Cl) \rightarrow \sigma^*(O_{34} - H_{39})$	13.84	0.74	0.091
	N_2-H_{33}….Cl	$LP(4)(Cl) \rightarrow \sigma^*(N_2 - H_{33})$	11.24	0.69	0.051
	N_4-H_{16}….Cl	$LP(3)(Cl) \rightarrow \sigma^*(N_4 - H_{16})$	17.98	0.71	0.068
	N_3-H_{15}….O	$LP(2)(O) \rightarrow \sigma^*(N_3 - H_{15})$	16.92	0.82	0.106
	N_1-H_{18}…. N_5	$LP(1)(N_5) \rightarrow \sigma^*(N_1 - H_{18})$	23.01	0.79	0.122
PHMB-DMSO	C_{34}-H_{35}….Cl	$LP(1)(Cl) \rightarrow \sigma^*(C_{34} - H_{35})$	3.84	0.97	0.013
	N_2-H_{33}….Cl	$LP(4)(Cl) \rightarrow \sigma^*(N_2 - H_{33})$	10.27	0.70	0.076
	N_4-H_{16}….Cl	$LP(3)(Cl) \rightarrow \sigma^*(N_4 - H_{16})$	8.82	0.73	0.069
	N_3-H_{15}….O	$LP(2)(O) \rightarrow \sigma^*(N_3 - H_{15})$	15.03	0.73	0.096
	N_1-H_{18}…. N_5	$LP(1)(N_5) \rightarrow \sigma^*(N_1 - H_{18})$	23.27	0.79	0.123
PHMB-H_2O	O_{34}-H_{36}….Cl	$LP(4)(Cl) \rightarrow \sigma^*(O_{34} - H_{36})$	27.87	0.73	0.093
	N_2-H_{33}….Cl	$LP(3)(Cl) \rightarrow \sigma^*(N_2 - H_{33})$	12.04	0.69	0.064
	N_4-H_{16}….Cl	$LP(3)(Cl) \rightarrow \sigma^*(N_4 - H_{16})$	8.98	0.72	0.066
	N_3-H_{15}….O	$LP(2)(O) \rightarrow \sigma^*(N_3 - H_{15})$	16.88	0.89	0.010
	N_1-H_{18}…. N_5	$LP(1)(N_5) \rightarrow \sigma^*(N_1 - H_{18})$	22.86	0.79	0.121

the solvent phase. The energy gap and electron potential in water solvent are larger than in other solvents. A large gap means high stability and low chemical reactivity. Therefore, the results confirm the stability of PHMB in water. While the N—H···Cl interaction in all complexes represented weak intermolecular interactions, it showed a steric effect in the biguanide pseudo-aromatic ring due to high repulsions. The results obtained using the AIM and NBO methods were consistent with each other. In addition, it was determined that PHMB was a non-toxic compound and did not bind to any defined protein.

CRediT authorship contribution statement

Sibel Çelik: Conceptualization, Data curation, Investigation, Methodology, Software, Supervision, Validation, Visualization, Writing – original draft. **Emine Tanış:** Conceptualization, Data curation, Methodology, Validation.

Declaration of Competing Interest

The authors declare that they have no known competing financial interests or personal relationships that could have appeared to influence the work reported in this paper.

Acknowledgements

Thanks are due to the Scientifc and Technological Research Council of Turkey (TUBITAK) for the use of its ULAKBIM/TRUBA high performance and grid computing center.

Funding

Not applicable.

Availability of data and material

Not applicable.

Code availability

The calculations were performed using Gaussian 09 program and Multiwfn and VMD software.

Authors' contributions

Sibel CELIK: Conceived and designed the experiments, software, analyzed data, and wrote the paper; Emine TANIS: Software analyzed, and interpreted the data, and wrote the paper.

References

[1] B. Roth, F.H.H. Brill, Polihexanide for wound treatment—how it began, Skin Pharmacol. Physiol. 23 (2010) 4–6.

[2] G.F. De Paula, G.I. Netto, L.H.C. Mattoso, Physical and chemical characterization of poly(hexamethylene biguanide) hydrochloride, Polymers 3 (2011) 928–941.

[3] E.E. Creppy, A. Diallo, S. Moukha, C. Eklu-Gadegbeku, D. Cros, Study of epigenetic properties of poly(hexamethylene biguanide) hydrochloride (PHMB), Int. J. Environ. Res. Public Health 11 (2014) 8069–8092.

[4] B.H. Mashat, Polyhexamethylene biguanide hydrochloride: features and applications, British J. Environ. Sci. 4 (2016) 49–55.

[5] U. Bernauer, Opinion of the scientific committee on consumer safety (SCCS) – 2nd Revision of the safety of the use of poly(hexamethylene) biguanide hydrochloride or polyaminopropyl biguanide (PHMB) in cosmetic products, Regul. Toxicol. Pharm. 73 (2015) 885–886.

[6] D. Wei, Q. Ma, Y. Guan, F. Hu, A. Zheng, X. Zhang, Z. Teng, H. Jiang, Structural characterization and antibacterial activity of oligoguanidine (polyhexamethylene guanidine hydrochloride), Mater. Sci. Eng., C 29 (2009) 1776–1780.

[7] J. Lorenzo-Morales, N.A. Khan, J. Walochnik, An update on Acanthamoeba keratitis: diagnosis, pathogenesis and treatment, Parasite (2015), https://doi.org/10.1051/parasite/2015010.

[8] F.C. Krebs, S.R. Miller, M.L. Ferguson, M. Labib, R.F. Rando, B. Wigdahl, Polybiguanides, particularly polyethylene hexamethylene biguanide, have activity against human immunodeficiency virus type 1, Biomed. Pharmacother. 59 (2005) 438–445.

[9] K. Kaehn, Polihexanide: a safe and highly effective biocide, Skin Pharmacol. Physiol. 23 (2010) 7–16.

[10] T. Ikeda, S. Tazuke, M. Watanabe, Interaction of biologically active molecules with phospholipid membranes, I. Fluorescence depolarization studies on the effect of polymeric biocide bearing biguanide groups in the main chain, BBA 735 (1983) 380–386.

[11] T. Ikeda, A. Ledwith, C.H. Bamford, R.A. Hann, Interaction of a polymeric bigunaide biocide with phospholipid membranes, BBA 769 (1984) 57–66.

[12] K. Moore, D. Gray, Using PHMB antimicrobial to prevent wound infection, Wounds UK 3 (2007) 96–102.

[13] A. Berg, O. Assadian, P. Rudolph, R.G. Mundkowski, J. Janda, A. Kramer, Intolerability to Lavasept peritoneal lavage in experimentally induced peritonitis in the guinea pig, Hygiene Medizin 33 (2008) 189–193.

[14] T. Eberlein, G. Haemmerle, M. Signer, U. Gruber-Moesenbacher, J. Traber, M. Mittlboeck, M. Abel, R. Strohal, Comparison of PHMB-containing dressing and silver dressings in patients with critically colonized or locally infected wounds, J Wound Care 21 (2012) 14–16.

[15] S. Ali, A.P.R. Wilson, Effect of pol-hexamethylene biguanide hydrochloride (PHMB) treated non-sterile medical gloves upon the transmission of *Streptococcus pyogenes*, carbapenem-resistant *E.coli*, MRSA and *Klebsiella pneumonia* from contact surfaces, BMC Infec Dis. (2017), https://doi.org/10.1186/s12879-017-2661-9.

[16] European Chemicals Agency (ECHA), Committee for Risk Assessment RAC. Opinion proposing harmonized classification and labeling at EU level Polyhexamethylene biguanide or Ply(hexamethylene) biguanide hydrochloride or PHMB. CLH-O-0000003799-56-03/F. Adopted 14.03.2014. http://echa.europa.eu.

[17] J.-E. Lee, B.S. Oum, H.Y. Choi, H.S. Yu, J.S. Lee, Cysticidal effect on Acanthamoeba and toxicity on human keratocytes by polyhexamethylene biguanide and chlorhexinide, Cornea 26 (2007) 736–741.

[18] A. Chowdhury, L.L. Arnold, Z. Wang, K.L. Pennington, P. Dodmane, A.P. Farragut-Cardosa, J.E. Klaunig, D. Cros, E.E. Creppy, S.M. Cohen, Effect of polyhexamethylene biguanide on rat liver, Toxicol. Lett. 285 (2018) 94–103.

[19] V. Christen, S. Faltermann, N.R. Brun, P.Y. Kunz, K. Fent, Cytotoxicity and molecular effects of biocidal disinfectants (quanternary ammonia, glutaraldehyde, poly(hexamethylene biguanide) hydrochloride PHMB) and their mixtures in vitro and in zebrafish eleuthero-embryos, Sci. Total Environ. 586 (2017) 1204–1218.

[20] A. Vedani, M. Dobler, Z. Hu, M. Smiesko, OpenVirtualToxLab – A platform for generating and exchanging in silico toxicity data, Toxicol. Lett. 232 (2015) 519–532.

[21] T. Pooventhiran, R. Thomas, Hydrogen bonds between valsartan and solvents (water and methanol): Evidences for solvation dynamics using local energy decomposition and abinitio molecular dynamics analysis, J. Mol. Liq. 354 (2022), 118856.

[22] T. Pooventhiran, B.S. Gangadharappa, O.A. Abu Ali, R. Thomas, D.I. Saleh, Study of the structural features and solvent effects using ab initio molecular dynamics and energy decomposition analysis of atogepant in water and ammonia, J. Mol. Liq. 352 (2022), 118672.

[23] M.J. Frisch, G.W. Trucks, H.B. Schlegel, G.E. Scuseria, M.A. Robb, J.R. Cheeseman, J.A. Montgomery, T. Vreven Jr., K.N. Kudin, J.C. Burant, J.M. Millam, S.S. Iyengar, J. Tomasi, V. Barone, B. Mennucci, M. Cossi, G. Scalmani, N. Rega, G.A. Petersson, H. Nakatsuji, M. Hada, M. Ehara, K. Toyota, R. Fukuda, J. Hasegawa, M. Ishida, T. Nakajima, Y. Honda, O. Kitao, H. Nakai, M. Klene, X. Li, J.E. Knox, H. P. Hratchian, J.B. Cross, V. Bakken, C. Adamo, J. Jaramillo, R. Gomperts, R. E. Stratmann, O. Yazyev, A.J. Austin, R. Cammi, C. Pomelli, J.W. Ochterski, P. Y. Ayala, K. Morokuma, G.A. Voth, P. Salvador, J.J. Dannenberg, V.G. Zakrzewski, S. Dapprich, A.D. Daniels, M.C. Strain, O. Farkas, D.K. Malick, A.D. Rabuck, K. Raghavachari, J.B. Foresman, J.V. Ortiz, Q. Cui, A.G. Baboul, S. Clifford, J. Cioslowski, B.B. Stefanov, G. Liu, A. Liashenko, P. Piskorz, I. Komaromi, R. L. Martin, D.J. Fox, T. Keith, M.A. Al-Laham, C.Y. Peng, A. Nanayakkara, M. Challacombe, P.M.W. Gill, B. Johnson, W. Chen, M.W. Wong, C. Gonzalez, J. A. Pople, Gaussian 03, Revision C.02, Gaussian, Wallingford, CT, 2004.

[24] A. Frisch, A.B. Nielsen, A.J. Holder, Gaussview Users Manuel, Gaussian Inc., Pittsburgh, 2001.

[25] S. Miertus, E. Scrocco, J. Tomasi, et al., Electrostatic interaction of a solute with a continuum. A direct utilization of AB initio molecular potentials for the prevision of solvent effect, Chem. Phys. 55 (1981) 117–129.

[26] R. Dennington, T. Keith, J. Millam, Gauss View, Version 5, Semichem Inc, ShawneeMission, KS, 2009.

[27] E.D. Glendening, A.E. Reed, J.E. Carpenter, F. Weinhold, NBO Version 3.1, TCI, University of Wisconsin, Madison, 1998.

[28] T. Lu, F. Chen, Multiwfn: a multifunctional wavefunction analyzer, J. Comput. Chem. 33 (2012) 580–592.

[29] T. Lu, F. Chen, Quantitative analysis of molecular surface based on improved Marching Tetrahedra algorithm, J. Mol. Graph. Model. 38 (2012) 314–323.

[30] W. Humphrey, A. Dalke, K. Schulten, VMD: visual molecular dynamics, J. Mol. Graph. 14 (1996) 33–38.

[31] A. Vedani, M. Dobler, M. Smiesko, VirtualToxLab – a platform for estimating the toxic potential of drugs, chemicals and natural products, Toxicol. Appl. Pharmacol. 261 (2012) 142–153.

[32] A.M. Rodrigues, S.Y.S. Silvaa, M.N. Oliveiraa, G.C.A. de Oliveira, A.L.F. Novais, G. F. de Paulaf, D.N. Souz, E.A. Belo, R. Gester, T. Andrade-Filhoa, Prediction of electronic and vibrational properties of poly (hexamethylene biguanide) hydrochloride: A combined theoretical and experimental investigation, J. Mol. Struct. 1246 (2021), 131176.

[33] S. Subashchandrabose, N. Ramesh Babu, H. Saleem, M., Syed Ali Padusha, Vibrational studies on (E)-1-((pyridine-2-yl)methylene)semicarbazide using experimental and theoretical method, J. Mol. Struct. 1094 (2015) 254–263.

[34] P. Larkin, Infrared and Raman Spectroscopy: Principles and Spectral Interpretation, Elsevier, 2017.

[35] S. Celik, S. Akyuz, A.E. Ozel, Vibrational spectroscopic and structural investigations of bioactive molecule Glycyl-Tyrosine (Gly-Tyr), Vib. Spectrosc. 92 (2017) 287–329.

[36] A.E. Ozel, S. Celik, S. Akyuz, Vibrational spectroscopic investigation of free and coordinated 5-aminoquinoline: The IR, Raman and DFT studies, J. Mol. Struct. 924–926 (2009) 523–530.

[37] S. Celik, S. Akyuz, A.E. Ozel, Vibrational spectroscopic characterization and structural investigations of Cepharanthine, a natural alkaloid, J. Mol. Struct. 1258 (2022), 132693.

[38] S. Subashchandrabose, A.R. Krishnan, H. Saleem, R. Parameswari, N. Sundaraganesan, V. Thanikachalam, G. Manikandan, Vibrational spectroscopic study and NBO analysis on bis(4-amino-5-mercapto-1,2,4-triazol-3-yl) methane using DFT method, Spectrochim. Acta, Part A 77 (2010) 877–884.

[39] M. Dilamian, M. Montazer, J. Masoumi, Antimicrobial electrospun membranes of chitosan/poly(ethylene oxide) incorporating poly(hexamethylene biguanide) hydrochloride, Carbohydr. Polym. 94 (2013) 364–371.

[40] G.-J. Zhao, K.-L. Han, Hydrogen bonding in the electronic excited state, Acc. Chem. Res. 45 (2011) 404–413.

[41] I. Fleming, Frontier Orbitals and Organic Chemical Reactions, Wiley, London, 1976.

[42] T. Koopmans, Physica 1 (1934) 104–113.

[43] P.K. Chattaraj, B. Maiti, HSAB principle applied to the time evolution of chemical reactions, J. Am. Chem. Soc. 125 (2003) 2705–2710.

[44] V. Arjunan, L. Devi, R. Subbalakshmi, T. Rani, S. Mohan, Spectrochim. Acta A 130 (2014) 164.

[45] M. Miar, A. Shiroudi, K. Pourshamsian, A. Reza Oliaey, F. Hatamjafari, J. Chem. Res. 45 (1) (2020) 147–158.

[46] S. Özkan Kotiloğlu, S. Çelik, E. Tanış, M. Kurban, ChemistrySelect 3 (2018) 5934–5940.

[47] P.L.A. Popelier, F.M. Aicken, S.E. O'Brien, Atoms in Molecules, an Introduction, Prentice Hall, 2000, pp. 143–198.

[48] I. Rozas, I. Alkorta, J. Elguero, Behavior of ylides containing N, O, and C atoms as hydrogen bond acceptors, J. Am. Chem. Soc. 122 (2000) 11154–11161.

[49] M. Tahenti, S. Gatfaoui, N. Issaoui, T. Roisnel, H. Marouani, J. Mol. Struct. 1207 (2020), 127781.

[50] Y.-Z. Zheng, Y. Zhou, Q. Liang, R. Da-Fu Chen, C.-L. Guo, X.u. Xi-J, Z.-N. Zhang, Z.-J. Huang, Dyes Pigm. 141 (2017) 179–187.

[51] J. Contreras-García, M. Calatayud, J.-P. Piquemal, J.M. Recio, Ionic interactions: comparative topological approach, Comput. Theor. Chem. 998 (2012) 193–201.
[52] A.E. Reed, L.A. Curtiss, F. Weinhold, Intermolecular interactions from a natural bond orbital, donor-acceptor viewpoint, Chem. Rev. 88 (1988) 899–926.
[53] O. Noureddine, S. Gatfaoui, S.A. Brandan, A. Sagaama, H. Marouani, N. Issaoui, Experimental and DFT studies on the molecular structure, spectroscopic properties, and molecular docking of 4-phenylpiperazine-1-ium dihydrogen phosphate, J. Mol. Struct. 1207 (2020), 127762.